arXiv:2404.01181v1 [astro-ph.HE] 1 Apr 2024

Constraining Dark Matter Annihilation with *Fermi*-LAT Observations of Ultra-Faint Compact Stellar Systems

Antonio Circiello,[1] Alex McDaniel,[1] Alex Drlica-Wagner,[2, 3, 4] Christopher Karwin,[5] Marco Ajello,[1] Mattia Di Mauro,[6] and Miguel Á. Sánchez-Conde[7, 8]

[1] *Department of Physics and Astronomy, Clemson University, Clemson, SC 29631, USA*
[2] *Fermi National Accelerator Laboratory, P.O. Box 500, Batavia, IL 60510, USA*
[3] *Kavli Institute for Cosmological Physics, University of Chicago, Chicago, IL 60637, USA*
[4] *Department of Astronomy and Astrophysics, University of Chicago, Chicago, IL 60637, USA*
[5] *NASA Postdoctoral Program Fellow, NASA Goddard Space Flight Center, Greenbelt, MD, 20771, USA*
[6] *Istituto Nazionale di Fisica Nucleare, Sezione di Torino, Via P. Giuria 1, 10125 Torino, Italy*
[7] *Instituto de Física Teórica UAM-CSIC, Universidad Autónoma de Madrid, C/ Nicolás Cabrera, 13-15, 28049 Madrid, Spain*
[8] *Departamento de Física Teórica, M-15, Universidad Autónoma de Madrid, E-28049 Madrid, Spain*

ABSTRACT

Recent results from numerical simulations and models of galaxy formation suggest that recently discovered ultra-faint compact stellar systems (UFCSs) in the halo of the Milky Way (MW) may be some of the smallest and faintest galaxies. If this is the case, these systems would be attractive targets for indirect searches of weakly interacting massive particle (WIMP) dark matter (DM) annihilation due to their relative proximity and high expected DM content. In this study, we analyze 14.3 years of gamma-ray data collected by the *Fermi*-LAT coincident with 26 UFCSs. No significant excess gamma-ray emission is detected, and we present gamma-ray flux upper limits for these systems. Assuming that the UFCSs are dark-matter-dominated galaxies consistent with being among the faintest and least massive MW dwarf spheroidal (dSphs) satellite galaxies, we derive the projected sensitivity for a dark matter annihilation signal. We find that observations of UFCSs have the potential to yield some of the most powerful constraints on DM annihilation, with sensitivity comparable to observations of known dSphs and the Galactic center. This result emphasizes the importance of precise kinematic studies of UFCSs to empirically determine their DM content.

1. INTRODUCTION

The Milky Way (MW) is surrounded by more than fifty dwarf spheroidal (dSph) satellite galaxies that reside in dark matter (DM) halos (e.g., Simon 2019, and references therein). While it was once possible to distinguish DM-dominated galaxies from DM-deficient star clusters based on size and luminosity (e.g., Willman et al. 2005), many recently discovered systems have sizes and luminosities that blur that boundary (see Cerny et al. 2023a, and references therein). In particular, dozens of ultra-faint compact stellar systems (UFCSs) have been discovered at distances of several tens of kpc possessing low luminosities, $L_\star < 10^4 L_\odot$, and small physical sizes, $r_h < 30\,\mathrm{pc}$ (see Table 1 for a list of references). Detailed kinematic studies of these systems are challenging due to their distances and low luminosities; however, recent theoretical arguments suggest that these systems could be the faintest and least massive DM-dominated galaxies (e.g., Manwadkar & Kravtsov 2022; Errani et al. 2023a). One example in this class

of systems is the recently discovered satellite Ursa Major III/UNIONS I (UMa III, Smith et al. 2023). While measurements of the velocity dispersion of this system are inconclusive due to the small number of measured stars, simulations suggest that a DM halo is necessary to stabilize the system against tidal dissolution (Errani et al. 2023b). If this system is indeed a DM-dominated galaxy, then galaxy–halo modeling arguments suggest that its host DM halo had a peak mass of $\lesssim 10^8 M_\odot$ (Sawala et al. 2015; Nadler et al. 2020; Manwadkar & Kravtsov 2022; Revaz 2023).[1]

If UFCSs are indeed DM-dominated galaxies, they would be powerful targets for searches for γ-ray emission from the annihilation of weakly interacting massive particles (WIMPs, for reviews, see Jungman et al. 1996; Bergström 2000; Abdo et al. 2010) DM. UFCSs are an

---

[1] This work is prefaced on the assumption that other UFCSs are similar in nature to UMa III and reside in DM subhalos of similar mass (see Sec. 2).

attractive target primarily due to their proximity, which could lead to a higher γ-ray flux from DM annihilation compared to the MW satellites studied previously. The detection of excess γ-ray emission coincident with one or more of these systems (especially the closest ones) would be exciting even if their DM contents have not yet been measured. On the other hand, a null detection of nearby DM-dominated UFCSs would increase the sensitivity of existing studies of dSphs, which already yield the most powerful and robust constraints on DM annihilation (McDaniel et al. 2023, and references therein).

In this Letter, we present the results of a search for γ-ray emission coincident with a sample of 26 UFCSs. Our sample was selected to be consistent with the galaxy size–luminosity relationship derived in Manwadkar & Kravtsov (2022). Our analysis of the *Fermi*-LAT γ-ray data adopts the procedure developed for the analysis of dSphs by McDaniel et al. (2023), which closely follows previous LAT analyses of dSphs (e.g., Ackermann et al. 2015; Albert et al. 2017). We find no significant excesses of γ-ray emission coincident with any of the UFCSs, and we present flux upper limits for each system. Under the assumption that the UFCSs are DM-dominated systems consistent with the known population of dSphs, we proceed to make projections for the ability to constrain the DM annihilation cross-section from the null detection of γ-ray emission. We also derive sensitivity projections for a subset of 17 out of the 26 UFCSs from the initial sample, applying a more stringent selection in size–luminosity space. We find that, although subject to large uncertainties at present, the DM cross-section upper limits derived under these assumptions for both samples of UFCSs are more sensitive than those obtained from recent dSphs analyses (e.g., Di Mauro et al. 2023; McDaniel et al. 2023), emphasizing the importance of kinematic studies of UFCSs to empirically determine their DM content.

The Letter is organized as follows. In Sec. 2 we discuss how our samples of UFCSs were selected. In Sec. 3 we detail the assumed model for the DM halos of UFCSs as well as the DM annihilation channels considered. Sec. 4 is devoted to the *Fermi*-LAT data selection and the analysis procedure. Finally, in Sec. 5, we discuss the results and conclude.

2. SAMPLE SELECTION

The populations of DM-dominated dSphs and DM-deficient classical globular clusters have historically been separable in the space of size (as indicated by the half-light radius) and luminosity (Fig. 1). However, as the sensitivity of optical imaging surveys has increased, fainter and more compact systems have been discovered

populating a region of parameter space where their classification is uncertain (e.g., Simon 2019; Drlica-Wagner et al. 2020). Furthermore, the low luminosities and distances of these systems make it difficult to measure the velocities of enough member stars to confidently determine velocity dispersions and dynamical masses. Early observational studies assumed that these systems were a low-luminosity tail of the globular cluster population, possibly formed and accreted within satellite galaxies that were subsequently disrupted (e.g., Mau et al. 2019). However, recent theoretical modeling work has suggested that the population of dwarf galaxies may extend to equivalently small sizes (e.g. Manwadkar & Kravtsov 2022; Errani et al. 2023a). In particular, the regulator model of galaxy formation developed in Kravtsov & Manwadkar (2022) and applied to simulations of a Milky-Way-like system in Manwadkar & Kravtsov (2022) predicts that a significant population of compact, low-luminosity satellite galaxies exists.

We select a sample of UFCSs that are consistent in physical size and absolute magnitude with the locus of galaxies produced by the model of Manwadkar & Kravtsov (2022, see their Fig. 12). In particular, we select UFCSs that have azimuthally averaged physical half-light radii $r_{1/2} < 30\,\mathrm{pc}$ and surface brightnesses of $24\,\mathrm{mag\,arcsec}^{-2} < \mu_V < 32\,\mathrm{mag\,arcsec}^{-2}$. Furthermore, we remove systems that have previously been included in population studies of γ-ray emission from dSphs (Bootes V, Cetus II, Draco II, Grus I, Leo Minor I, Pictor I, Segue 1, Segue 3, Triangulum II, Tucana V, Virgo II, and Willman 1) (e.g., Albert et al. 2017; McDaniel et al. 2023), or have been confirmed to be DM-deficient from kinematic measurements (AM 4, Palomar 5, Palomar 13, Palomar 14; Harris 1996, 2010 edition). We apply the same selection criteria used for the dSphs in McDaniel et al. (2023) to avoid contamination from other sources of γ-ray emission by checking if any targets in our sample fall within the 95% confidence radius of a 4FGL-DR4 source, or within $0.1°$ (i.e., roughly the mean of the 95% confidence radius of point sources in the 4FGL, Ballet et al. 2023) of a source in the BZCat, CRATES, and WIBRaLS catalogs. No targets were removed by this criteria. We refer to UFCSs passing this selection as the 'inclusive sample', which contains 26 targets (Table 1). We also analyze a subset of this sample, selecting targets in a more restrictive range of surface brightness ($25\,\mathrm{mag\,arcsec}^{-2} < \mu_V < 32\,\mathrm{mag\,arcsec}^{-2}$), which corresponds to the region of maximum density of galaxies predicted by Manwadkar & Kravtsov (2022). We refer to this selection as our 'nominal sample', which contains 17 of the 26 UFCSs from the inclusive sample. Targets
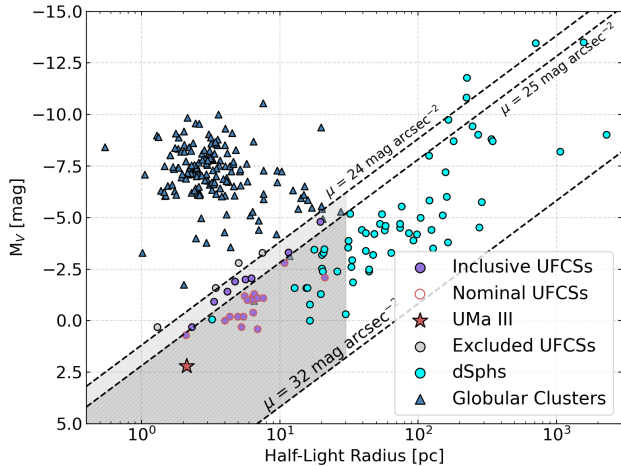
Figure 1. V-band absolute magnitude vs. physical half-light radius for Milky Way globular clusters, dSphs, and UFCSs. The dashed lines mark the minimum surface brightness used to select the inclusive ($\mu > 24 \, \mathrm{mag \, arcsec^{-2}}$) and nominal ($\mu > 25 \, \mathrm{mag \, arcsec^{-2}}$) samples, based on the model of Man-wadkar & Kravtsov (2022). The light and dark grey shaded areas represent the regions of inclusive and nominal selections, respectively. The purple points are the UFCSs in the inclusive sample. The UFCSs that are also included in the nominal sample are circled in red. A complete list of both samples is reported in Table 1. The grey points are the UFCSs that fall outside our selections and were excluded from the analysis for this reason. The cyan points are the confirmed dSphs from `dmsky` (https://github.com/fermiPy/dmsky). The dark blue triangles are the confirmed globular clusters from the Local Volume Database (Pace 2024).

that fall into this selection are listed separately in Table 1.

3. DARK MATTER ANNIHILATION

Astrophysical searches for DM involve looking for the signatures of DM interactions. In the WIMP DM model, one possible signature of DM annihilation is γ-ray emission through the production of high-energy standard model particles (e.g., Bertone et al. 2005, for a review). The expected γ-ray flux from DM annihilation is (Bergström et al. 1998):

$$\frac{d\Phi_\chi}{dE} = J \times \frac{1}{4\pi} \frac{\langle \sigma v \rangle}{2M_\chi^2} \sum_i \beta_i \frac{dN_i}{dE}, \qquad (1)$$

where M_χ is the rest mass of the DM particle, and $\langle \sigma v \rangle$ is the velocity-averaged DM annihilation cross-section. The sum is performed over the annihilation channels, where β_i is the branching ratio for the i-th channel. The γ-ray spectrum per annihilation event given the annihilation channel, dN/dE, is given by the DM model that is being considered. In this work, we use the

PPPC4DMID[2] tables from Cirelli et al. (2011) to compute the different annihilation spectra. The annihilation channels considered are $b\bar{b}$ and $\tau^+\tau^-$.[3] These two annihilation channels are typically chosen as representative because their spectra enclose most of the shapes of the other annihilation channels (Cirelli et al. 2011). Electroweak corrections are taken into account only for the $\tau^+\tau^-$ channel, as they have a minimal effect in the $b\bar{b}$ channel (Ciafaloni et al. 2011). The 'J-factor' (J) is a geometrical quantity obtained by integrating the squared density (ρ_χ^2) of DM along the line of sight (l.o.s., ℓ) and the solid angle ($\Delta\Omega$)

$$J = \int_{\Delta\Omega} \int_{\mathrm{l.o.s.}} \rho_\chi^2 \, d\ell \, d\Omega. \qquad (2)$$

While the DM density profile of a system can be inferred from a dynamical Jeans analysis of its member stars (e.g., Bonnivard et al. 2015; Pace & Strigari 2019), spectroscopic measurements are currently unavailable for many faint systems, making a direct determination of the J-factor impossible. Several previous γ-ray studies (e.g., Drlica-Wagner et al. 2015; Albert et al. 2017; Mc-Daniel et al. 2023) have estimated the J-factors for targets that lacked direct measurements through scaling relations with the kinematic or photometric properties of the system (e.g., Drlica-Wagner et al. 2015; Evans et al. 2016; Pace & Strigari 2019). In this analysis, we use the most recent versions of these relations from Pace & Strigari (2019),

$$\frac{J_{\mathrm{photo}}(0.5°)}{\mathrm{GeV^2 \, cm^{-5}}} \simeq 10^{18.17} \left(\frac{L_V}{10^4 L_\odot}\right)^{0.23} \left(\frac{d}{100 \, \mathrm{kpc}}\right)^{-2} \left(\frac{r_{1/2}}{100 \mathrm{pc}}\right)^{-1} \qquad (3)$$

to estimate the J-factor from photometric properties. In this equation, d is the distance to the system, $r_{1/2}$ is the azimuthally-averaged physical half-light radius, and L_V is the V-band luminosity. Since none of the targets in our sample have confidently measured velocity dispersions, the J-factors used in this analysis are computed from Eq. 3 with the exception of UMa III, for which we use the value obtained by Crnogorčević & Linden (2023) from the velocity dispersion scaling relation from Pace & Strigari (2019), rather than the photometric one in Eq. 3.

In previous dSph analyses (e.g., Albert et al. 2017; McDaniel et al. 2023), the uncertainty on the J-factors estimated this way is assumed to be 0.6 dex, to represent the expected measurement uncertainty after kinematic observations. For the UFCSs, this choice may be less

---

[2] http://www.marcocirelli.net/PPPC4DMID.html

[3] In a recent work by Arina et al. (2023) the authors have computed updated source spectra for γ-rays from dark matter, which for the annihilation channels used in this paper are similar to the one obtained in the PPPC4DMID.
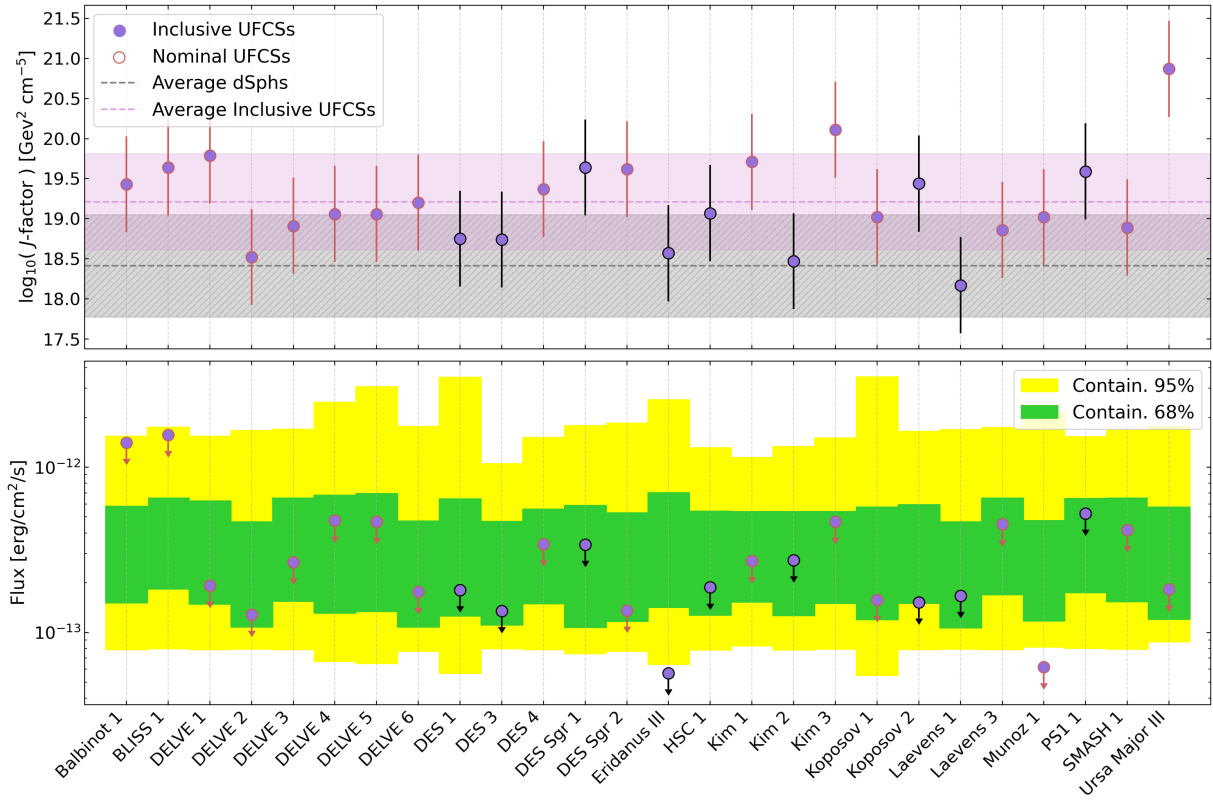
Figure 2. Top: *J*-factor for the selected UFCSs derived using the scaling relations of Pace & Strigari (2019). We use the photometric *J*-factor relation (Eq. 3) for all the sources except UMa III, which is instead derived from the velocity dispersion scaling relation of Pace & Strigari (2019) as reported by Crnogorčević & Linden (2023). We included the average *J*-factors, with their uncertainties, for the dSphs (grey band) and the inclusive sample of UFCSs (purple band) **Bottom:** γ-ray flux upper limits in the [0.5 GeV - 1 TeV] energy band at 95% confidence level for the selected UFCSs. The green and yellow containment bands are obtained by selecting blank fields that reside at the same Galactic latitude as each target (within ± 5°).

conservative, since the faintness of some of these systems will likely increase the statistical uncertainty of kinematic measurements. However, Albert et al. (2017) found that changing the assumed *J*-factor uncertainty had a small effect compared to the uncertainty arising from the unknown nature of the UFCSs (i.e., some may be devoid of DM), which we discuss in more detail in Sec. 5. Consequently, we adopt the value for the *J*-factor uncertainty of 0.6 dex assumed in Albert et al. (2017) and McDaniel et al. (2023), to allow for a direct comparison with the limits derived from the dSphs. In Fig. 2 we show the assumed *J*-factors and assumed uncertainties for each target in our sample.

4. *Fermi*-LAT DATA ANALYSIS

We analyze data from the *Fermi*-Large Area Telescope (LAT; Atwood et al. 2009; Ajello et al. 2021) taken between August 4, 2008 and December 1, 2022 (14.3 years). Our data set and analysis pipeline closely follows the dSph analysis performed by McDaniel et al. (2023), which makes use of the `Fermitools` (v2.2.0) via the `fermipy` (v1.2) interface (Wood et al. 2017). Photons

from the P8R3_SOURCE_V3 class are selected with energies between 500 MeV and 1 TeV. Events observed at an angle from the zenith of the spacecraft greater than 100° are removed to avoid contamination from Earth's limb. Data from all four point spread function (PSF) event classes are selected and used in a joint-likelihood analysis. This approach splits the photon events into PSF classes and includes additional information about the event-wise quality of the angular reconstruction and uses dedicated instrument response functions for each PSF event class (Ackermann et al. 2015).

The first step of the analysis is to define a 10° × 10° region of interest (ROI) centred on each UFCS target. Events are divided into eight logarithmically spaced bins of energy and spatial bins of 0.08°. The ROI is modeled including the Galactic diffuse emission (`gll_iem_v07.fits`), the isotropic spectrum for the PSF type that is being considered (`iso_P8R3_SOURCE_V3_PSF{`i`}_v1.txt`, with i going from 0 to 3) and point-like and extended sources from the 4FGL-DR3 (`gll_psc_v29.fits`, Abdollahi et al.

2020, 2022). In particular, all sources that are up to 15° from the target are included to account for γ-ray emission originating outside the ROI. Each UFCS target is modeled as a point-like source with a power-law spectrum. These assumptions were made to allow for a close comparison to the dSph results from Mc-Daniel et al. (2023). Previous studies on the effects of the spatial extension of targets on DM limits have been performed for the dSphs, and have shown that modeling the sources as extended can lead to weaker limits in the DM parameter space (Di Mauro et al. 2022). However, this additional uncertainty is subdominant to the uncertainty coming from our lack of knowledge of the DM density profile of each UFCS in the sample. The model is optimized keeping as free parameters the photon index and normalization of the Galactic diffuse emission and the normalization of the isotropic component, as well as the normalization of all sources with test statistics[4] TS ≥ 25 that are up to 5° away from the target, and the normalization and photon index of all sources with TS ≥ 500 that are up to 7° away from the target. The `find_sources()` method is used to look for additional sources in the ROI and if any is found with TS > 16, it is included in the model. The new sources closest to a target, both with TS ∼ 20, are found with an offset of 0.51° and 0.22° from DELVE 2 and DELVE 3, respectively[5]. Neither source overlaps with the target within their 95% localization countour (∼ 0.1°). All the other new sources are found at an offset > 1°. The next step in the analysis is to calculate the spectral energy distribution (SED) for each target through the use of the `fermipy sed()` function (for more information on this method, see Ackermann et al. 2014). Fits are performed independently in each energy bin, with the target modeled by a power-law spectrum with a fixed index of 2 and free normalization, while leaving the diffuse background normalizations free to vary. This procedure yields a likelihood profile, $\mathcal{L}(d\Phi_\gamma/dE, E)$, in flux–energy space. The likelihood for a given DM mass and cross-section can be then computed by replacing $d\Phi_\gamma/dE$ with the theoretical γ-ray yield from DM annihilation (Eq. 1) – which is a function of DM mass, cross-section and energy – then summing over energy bins. This can be summarized by

the following expression:

$$\mathcal{L}(\langle\sigma v\rangle, M_\chi) = \sum_{E_i} \mathcal{L}\left[\frac{d\Phi_\chi}{dE}(\langle\sigma v\rangle, M_\chi, E_i), E_i\right], \quad (4)$$

This likelihood profile is used to define a TS profile for the target,

$$\text{TS}(\langle\sigma v\rangle, M_\chi) = 2\left[\frac{\mathcal{L}(\langle\sigma v\rangle, M_\chi)}{\mathcal{L}_0}\right], \quad (5)$$

where $\mathcal{L}_0$ is the likelihood for the null hypothesis (i.e., no γ-ray source). The parameter space considered covers a mass range of $M_\chi \in [5; 10^4]$ GeV and a cross-section range of $\langle\sigma v\rangle \in [10^{-28}; 10^{-22}]$ cm³s⁻¹, which is motivated by GeV–TeV scale thermal relic WIMP DM models and the constraining capability of *Fermi*-LAT observations. To incorporate uncertainties in the J-factors the *Fermi*-LAT likelihood function is multiplied by a J-factor likelihood function, $\mathcal{L}_J$:

$$\mathcal{L}_J(J) = \frac{1}{\ln(10)\sqrt{2\pi}\sigma_J J_{obs}}$$
$$\times \exp\left[-\left(\frac{\log_{10}(J) - \log_{10}(J_{obs})}{\sqrt{2}\sigma_J}\right)^2\right]. \quad (6)$$

The J-factor likelihood function is defined as a Gaussian in the log J space, where J_{obs} is the J-factor value estimated from the scaling relations in Pace & Strigari (2019), and σ_J is the uncertainty on the J-factor, assumed to be 0.6 dex in this analysis.

The limits obtained from the γ-ray data coincident with UFCSs can be compared to statistical expectations of the background using a 'blank-field' analysis (e.g., Ackermann et al. 2014). The analysis of blank fields accounts for the effects of undetected sources in the *Fermi*-LAT data and for the uncertainty in the models of the diffuse background emission by sampling of regions of the sky that contain no known γ-ray sources or likely γ-ray emitters based on spatial coincidence with the *Fermi*-LAT and multiwavelength catalogs. The blank fields are randomly selected at high Galactic latitude ($|b| > 15°$) by applying similar criteria to those used to select the sample of UFCSs—i.e., excluding regions centered within the 95% confidence radius of a 4FGL-DR3 source or within 0.1° from any source in the BZCat, CRATES, and WIBRaLS catalogs. We use the same 1000 regions selected for the dSphs analysis in McDaniel et al. (2023).[6] From these regions, sets of 26 blank fields (i.e., the same size as the UFCS sample) are randomly

---

[4] The TS of the sources is defined as TS = $2\log(\mathcal{L}/\mathcal{L}_0)$, where $\mathcal{L}$ is the likelihood derived including the target of interest in the model fit, and $\mathcal{L}_0$ is the likelihood of the null hypothesis (i.e., fixing the flux of the target source at zero).

[5] Including or removing DELVE 3 from the analysis has negligible effects on the combined constraints.

[6] The data are taken from the public figshare page: https://figshare.com/articles/dataset/24058650

selected without replacement 10^4 times to perform a combined blank-field analysis. We refer to McDaniel et al. (2023) for more details on the blank-field analysis.

5. RESULTS AND DISCUSSION

We analyzed ~15 years of γ-ray from *Fermi*-LAT data coincident with a selection of UFCSs that are potentially DM dominated. If their nature is confirmed, the UFCSs are expected to put stringent constraints on DM properties, since their relative proximity could lead to a higher flux of γ-rays from DM annihilation compared to the previously studied dSphs. However, no significant γ-ray emission is observed in the combined sample of UFCSs. We present the upper limits for the γ-ray flux from each source in Fig. 2, with the respective values reported in Tab. 1.

To assess the significance of a signal from the individual targets in our sample, we evaluate the maximum TS over all cross-section values as a function of the mass and compare it to the 84% and 97.5% containment bands from the 1000 individual blank fields (see Fig. 3). Only DELVE 4 and BLISS 1 (colored lines in Fig. 3) show local significance $\gtrsim 2\sigma$ over the background, though we notice that these peaks in significance occur in different ranges of M_χ, which would not be expected if they could both be attributed purely to DM annihilation.

We derive the sensitivity to the null detection of γ-ray emission in UFCSs to put constraints on DM properties in the velocity-averaged cross-section vs. mass space, for the $b\bar{b}$ and $\tau^+\tau^-$ annihilation channels. In Fig. 4 we compare the upper limits obtained from the UFCSs in the inclusive and nominal samples for both channels to the results for dSphs (McDaniel et al. 2023), for the Galactic center excess (GCE, Calore et al. 2015; Di Mauro 2021), and to the cross-section for thermal relic DM (Steigman et al. 2012). The sensitivities obtained from the two selections are similar, with the nominal sample yielding a slightly less stringent constraint. We also present the results obtained excluding UMa III from the nominal sample, since this source dominates the sample due to its proximity and high J-factor. Crnogorčević & Linden (2023) have demonstrated that, according to the current estimation of its J-factor, UMa III alone can put constraints on DM properties that are competitive with the most recent results from dSphs. In this context, evaluating the effects of excluding this target from the sample is crucial for two reasons. First, it gives an upper limit on how the results presented here would be affected if further investigation of UMa III leads to a lower estimation of its J-factor. Secondly, it evaluates the contribution to the constraints from the remaining targets of the nominal sample, showing

that they provide a pronounced improvement to the constraints relative to the dSphs. The upper limits obtained from both the inclusive and nominal samples are better than the constraints obtained from previous analyses at all masses and in both channels. Even with the exclusion of UMa III, the limits obtained from the nominal sample are lower than the dSphs constraints for the majority of the mass range. We also take into account the effects of the background through the combined blank-field analysis, from which we derive the 68% and 95% containment bands in the top panels of Fig 4. The UFCSs limits are mostly contained within these bands, and the only slight excess is observed at the highest masses in the $b\bar{b}$ channel when UMa III is excluded from the analysis (Fig 4).

As said, our analysis is premised on the assumption that the UFCSs are DM-dominated. Yet, given the lack of direct spectroscopic measurements, the DM content of these systems cannot be confirmed at present, and it is possible that some of these systems are DM-deficient star clusters. To account for the possibility that not all of the systems are hosted in DM halos, we also compute the sensitivity for random subsets of the UFCSs in the inclusive sample, effectively treating the excluded systems as devoid of DM. This allows us to gauge the main source of uncertainty on the results, which comes from the undetermined nature of the targets in our sample.

In the bottom panels of Fig. 4, we compute the constraints for 1000 subsets of 13 UFCSs selected randomly from the 26 UFCSs in the inclusive sample. This allows us to evaluate the variability of the results due to the exclusion of some of the sources. We highlight the selections that contain UMa III as these tend to lead, on average, to better constraints compared to the selections that do not contain this system. Again, we compare these bands to results for the dSphs and the GCE, as well as the thermal relic cross-section. In the $b\bar{b}$ channel the selections that do not include UMa III are similar to the results from the dSphs, with their average being more constraining up to high values of the DM mass ($M_\chi \gtrsim 1$ TeV). In the $\tau^+\tau^-$ channel, this inversion happens at about an order of magnitude lower mass ($M_\chi \sim 100$ GeV), yet once again when considering the variability coming from the different selections, the constraints are compatible. In both channels, most of the DM limits from selections that include UMa III are still better than the dSphs constraints, and their average is comparable to the limits obtained from the nominal sample. A similar comparison can be done with observations of the GCE, which lie close to the average constraint of the selections that include UMa III.
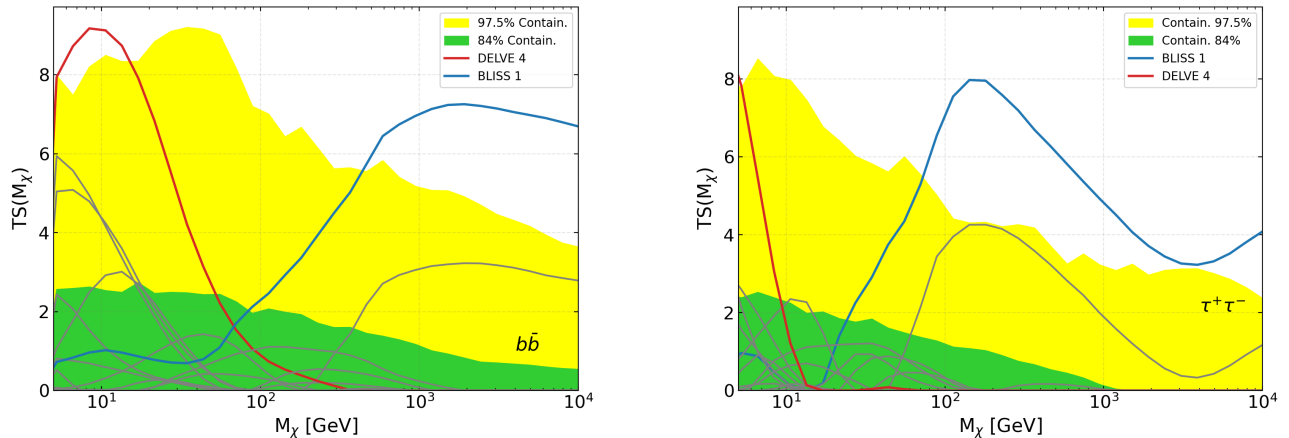
Figure 3. Maximum TS over all cross-section values vs. Mass for the individual UFCSs in the $b\bar{b}$ (**left**) and $\tau^+\tau^-$ (**right**) channels. The colored lines highlight the targets that show a TS excess over the 97.5% and 84% containment regions for the individual blank fields (green and yellow bands).

This study highlights the need for further investigations of the nature of UFCSs, since confirming that even a few of the observed systems are hosted in DM halos could significantly increase the sensitivity of studies on DM annihilation. Furthermore, optical imaging surveys such as DELVE (Drlica-Wagner et al. 2021), UNIONS (Ibata et al. 2017), and Rubin LSST (Ivezić et al. 2019) are likely to discover more UFCSs (e.g., Hargis et al. 2014; Nadler et al. 2020; Manwadkar & Kravtsov 2022). On-going spectroscopic observing campaigns with the Keck and Magellan telescopes, as well as with the Dark Energy Spectroscopic Instrument (DESI, DESI Collaboration et al. 2016), should be able to provide initial kinematic measurements following procedures similar to those described in Simon (2019); however, comprehensive measurements of the DM content of very faint systems will likely require 30-meter class telescopes (e.g., Cypriano et al. 2018).

Software: numpy, scipy, astropy, Fermitools, fermiPy (Wood et al. 2017), dmsky,[7] local_volume_database,[8]

---

[7] https://github.com/fermiPy/dmsky

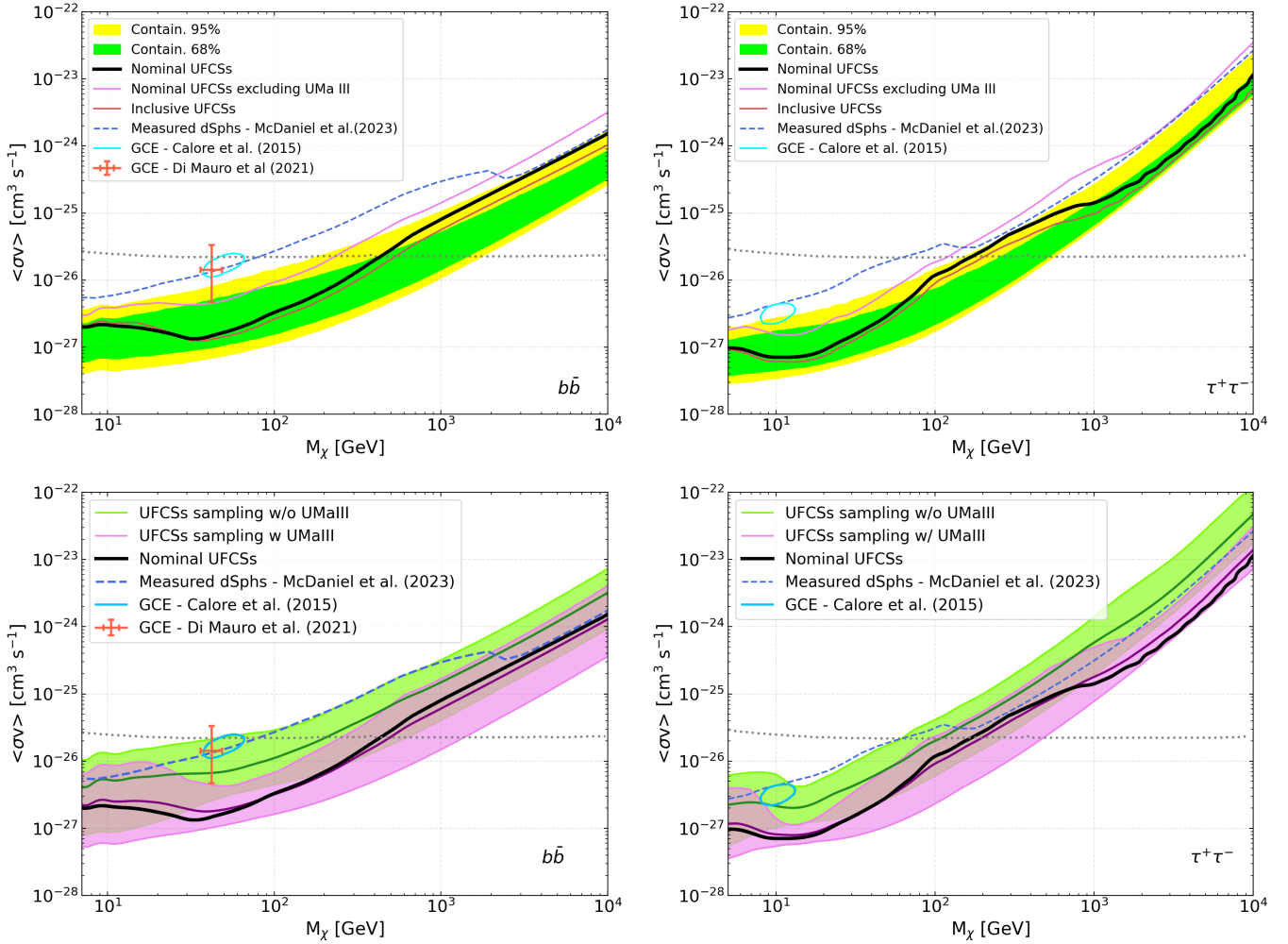[8] https://github.com/apace7/local_volume_database

Figure 4. Top: Sensitivity of *Fermi*-LAT observations of UFCSs to DM annihilation via the $b\bar{b}$ (**left**) and $\tau^+\tau^-$ (**right**) channels. The solid black lines represent the constraints obtained from the combined analysis of the UFCSs in the nominal sample. The pink lines are constraints obtained excluding UMa III from this selection. The red lines are the constraints obtained from the combined analysis of UFCSs in the inclusive sample. The yellow and green regions are, respectively, the 95% and 68% containment bands obtained from the combined analysis of 1000 blank-fields. The dotted line is the thermal relic cross-section from Steigman et al. (2012). The dashed blue lines are constraints from McDaniel et al. (2023) for the measured sample of dSphs. The light blue profile represents the DM interpretation of the GCE from Calore et al. (2015), while the red point with error bars is the GCE measurement from Di Mauro & Winkler (2021)
Bottom: Sensitivity of *Fermi*-LAT observations to DM annihilation via the $b\bar{b}$ (**left**) and $\tau^+\tau^-$ (**right**) channels derived by randomly selecting half of the UFCSs in the inclusive sample. The green band represents the selections that do not include UMa III, while the pink band represents the selections that include this source. The solid lines represent the average constraint from the respective band of the same color. The solid black line represents the constraints from the nominal sample of UFCSs. We also include results from previous analyses on the dSphs (McDaniel et al. 2023) and GCE (Calore et al. 2015; Di Mauro & Winkler 2021).

REFERENCES

Abdo, A. A., Ackermann, M., Ajello, M., et al. 2010, The Astrophysical Journal, 712, 147. https://dx.doi.org/10.1088/0004-637X/712/1/147

Abdollahi, S., Acero, F., Ackermann, M., et al. 2020, The Astrophysical Journal Supplement Series, 247, 33. https://dx.doi.org/10.3847/1538-4365/ab6bcb

Abdollahi, S., Acero, F., Baldini, L., et al. 2022, The Astrophysical Journal Supplement Series, 260, 53. https://dx.doi.org/10.3847/1538-4365/ac6751

Ackermann, M., Albert, A., Anderson, B., et al. 2014, PhRvD, 89, 042001

Ackermann, M., Albert, A., Anderson, B., et al. 2015, Phys. Rev. Lett., 115, 231301. https://link.aps.org/doi/10.1103/PhysRevLett.115.231301

Ajello, M., Atwood, W. B., Axelsson, M., et al. 2021, ApJS, 256, 12

Albert, A., Anderson, B., Bechtol, K., et al. 2017, The Astrophysical Journal, 834, 110. https://dx.doi.org/10.3847/1538-4357/834/2/110

Arina, C., Di Mauro, M., Fornengo, N., et al. 2023, arXiv:2312.01153

Atwood, W. B., Abdo, A. A., Ackermann, M., et al. 2009, ApJ, 697, 1071

Balbinot, E., Santiago, B. X., da Costa, L., et al. 2013, ApJ, 767, 101

Ballet, J., Bruel, P., Burnett, T. H., Lott, B., & The Fermi-LAT collaboration. 2023, arXiv e-prints, arXiv:2307.12546

Bergström, L. 2000, Reports on Progress in Physics, 63, 793

Bergström, L., Ullio, P., & Buckley, J. H. 1998, Astroparticle Physics, 9, 137

Bertone, G., Hooper, D., & Silk, J. 2005, PhR, 405, 279

Bonnivard, V., Combet, C., Daniel, M., et al. 2015, MNRAS, 453, 849

Calore, F., Cholis, I., McCabe, C., & Weniger, C. 2015, Phys. Rev. D, 91, 063003. https://link.aps.org/doi/10.1103/PhysRevD.91.063003

Cerny, W., Drlica-Wagner, A., Li, T. S., et al. 2023a, ApJL, 953, L21

Cerny, W., Martínez-Vázquez, C. E., Drlica-Wagner, A., et al. 2023b, ApJ, 953, 1

Ciafaloni, P., Comelli, D., Riotto, A., et al. 2011, Journal of Cosmology and Astroparticle Physics, 2011, 019. https://dx.doi.org/10.1088/1475-7516/2011/03/019

Cirelli, M., Corcella, G., Hektor, A., et al. 2011, JCAP, 2011, 051

Conn, B. C., Jerjen, H., Kim, D., & Schirmer, M. 2018, ApJ, 852, 68

Crnogorčević, M., & Linden, T. 2023, arXiv e-prints, arXiv:2311.14611

Cypriano, E., Drlica-Wagner, A., Freedman, W., et al. 2018, in Giant Magellan Telescope Science Book. https://www.staging.giantmagellan.org/wp-content/uploads/2021/11/GMTScienceBook2018.pdf

DESI Collaboration, Aghamousa, A., Aguilar, J., et al. 2016, arXiv e-prints, arXiv:1611.00036

Di Mauro, M. 2021, PhRvD, 103, 063029

Di Mauro, M., Pérez-Romero, J., Sánchez-Conde, M. A., & Fornengo, N. 2023, Phys. Rev. D, 107, 083030. https://link.aps.org/doi/10.1103/PhysRevD.107.083030

Di Mauro, M., Stref, M., & Calore, F. 2022, Phys. Rev. D, 106, 123032

Di Mauro, M., & Winkler, M. W. 2021, Phys. Rev. D, 103, 123005. https://link.aps.org/doi/10.1103/PhysRevD.103.123005

Drlica-Wagner, A., Albert, A., Bechtol, K., et al. 2015, The Astrophysical Journal Letters, 809, L4. https://dx.doi.org/10.1088/2041-8205/809/1/L4

Drlica-Wagner, A., Bechtol, K., Mau, S., et al. 2020, ApJ, 893, 47

Drlica-Wagner, A., Carlin, J. L., Nidever, D. L., et al. 2021, ApJS, 256, 2

Errani, R., Ibata, R., Navarro, J. F., Peñarrubia, J., & Walker, M. G. 2023a, arXiv e-prints, arXiv:2311.14798

Errani, R., Navarro, J. F., Smith, S. E. T., & McConnachie, A. W. 2023b, arXiv e-prints, arXiv:2311.10134

Evans, N. W., Sanders, J. L., & Geringer-Sameth, A. 2016, PhRvD, 93, 103512

Hargis, J. R., Willman, B., & Peter, A. H. G. 2014, ApJL, 795, L13

Harris, W. E. 1996, AJ, 112, 1487

Homma, D., Chiba, M., Komiyama, Y., et al. 2019, PASJ, 71, 94

Ibata, R. A., McConnachie, A., Cuillandre, J.-C., et al. 2017, ApJ, 848, 128

Ivezić, Ž., Kahn, S. M., Tyson, J. A., et al. 2019, ApJ, 873, 111

Jungman, G., Kamionkowski, M., & Griest, K. 1996, PhR, 267, 195

Kim, D., & Jerjen, H. 2015, ApJ, 799, 73

Table 1. List of the UFCSs that fall in the selection regions highlighted in 1. The nominal sample includes the sources that fall below the surface brightness line $\mu = 25$ mag arcsec^{-2}. The inclusive sample contains all the sources in the nominal sample, with the addition of the sources in the region corresponding to 24 mag arcsec$^{-2} < \mu \leq 25$ mag arcsec^{-2}. The values of the J-factor listed here are computed using the photometric scaling relation in Eq. 3 (Pace & Strigari 2019) for all systems except UMa III, where we adopt the value evaluated by Crnogorčević & Linden (2023). The J-factors and the upper limits for γ-ray flux at 95% confidence level in the [0.5 GeV - 1 TeV] energy range for each source are reported in Fig. 2. While we report the main reference for each source in the last column, refer to the Local Volume Database (Pace 2024) for a more complete list.

Name	GLon	GLat	Distance	$R_{1/2}$	M_V	$\log_{10}(J_{photo})$	F_{UL}	Ref.
	[°]	[°]	[kpc]	[pc]		[GeV^2/cm^5]	[$\times 10^{-12}$ erg/cm^2/s]	
Nominal sample								
Balbinot 1	75.18	-32.64	31.9	5.57	-1.2	19.43	14.07	Balbinot et al. (2013)
BLISS 1	290.83	19.65	23.7	4.14	0.0	19.64	15.68	Mau et al. (2019)
DELVE 1	14.19	30.29	19.0	6.08	-0.2	19.79	1.92	Mau et al. (2020)
DELVE 2	294.24	-47.79	71.0	21.48	-2.1	18.52	1.28	Cerny et al. (2023b)
DELVE 3	335.85	-27.06	56.0	6.52	-1.3	18.91	2.66	Cerny et al. (2023b)
DELVE 4	42.31	56.43	45.0	6.41	-0.2	19.06	4.76	Cerny et al. (2023b)
DELVE 5	19.38	61.36	39.0	7.71	0.4	19.06	4.68	Cerny et al. (2023b)
DELVE 6	290.57	-49.08	79.8	0.43	-1.2	15.61	1.76	Cerny et al. (2023a)
DES 4	270.87	-33.44	31.3	7.56	-1.1	19.37	3.43	Torrealba et al. (2019)
DES Sgr 2	163.58	-52.20	23.8	11.04	-1.1	19.62	1.36	Luque et al. (2017)
Kim 1	68.52	-38.42	19.8	6.91	0.3	19.71	2.71	Kim & Jerjen (2015)
Kim 3	310.86	31.79	15.1	2.29	0.7	20.11	4.69	Kim et al. (2016)
Koposov 1	260.97	70.76	48.3	8.71	-1.0	19.02	1.58	Muñoz et al. (2018)
Laevens 3	63.60	-21.18	61.4	11.43	-2.8	18.86	4.53	Longeard et al. (2019)
Munoz 1	105.44	45.58	45.0	6.41	-0.4	19.02	0.62	Muñoz et al. (2018)
SMASH 1	292.14	-27.99	57.0	9.45	-1.0	18.89	4.18	Martin et al. (2016)
Ursa Major III	194.61	73.68	10.0	3.0	2.2	20.87	1.83	Smith et al. (2023)
Inclusive sample								
DES 1	310.52	-67.83	76.0	5.42	-1.4	18.75	1.81	Conn et al. (2018)
DES 3	343.83	-46.51	76.2	6.21	-2.0	18.74	1.35	Luque et al. (2018)
DES Sgr 1	142.83	-75.79	26.5	2.71	0.3	19.64	3.40	Luque et al. (2017)
Eridanus III	274.95	-59.60	91.0	8.34	-2.0	18.57	0.57	Conn et al. (2018)
HSC 1	66.32	-41.84	46.0	5.89	-0.2	19.07	1.87	Homma et al. (2019)
Kim 2	347.15	-42.07	100.0	13.96	-3.3	18.47	2.74	Kim et al. (2015)
Koposov 2	195.11	25.55	34.7	4.44	-0.9	19.44	1.52	Muñoz et al. (2018)
Laevens 1	274.81	47.85	145.0	21.51	-4.8	18.17	1.67	Laevens et al. (2014)
PS1 1	10.04	-17.42	29.6	4.74	-1.9	19.59	5.25	Torrealba et al. (2019)

Kim, D., Jerjen, H., Mackey, D., Costa, G. S. D., & Milone, A. P. 2016, The Astrophysical Journal, 820, 119. https://dx.doi.org/10.3847/0004-637X/820/2/119

Kim, D., Jerjen, H., Milone, A. P., Mackey, D., & Da Costa, G. S. 2015, ApJ, 803, 63

Kravtsov, A., & Manwadkar, V. 2022, MNRAS, 514, 2667

Laevens, B. P. M., Martin, N. F., Sesar, B., et al. 2014, ApJL, 786, L3

Longeard, N., Martin, N., Ibata, R. A., et al. 2019, MNRAS, 490, 1498

Luque, E., Pieres, A., Santiago, B., et al. 2017, MNRAS, 468, 97

Luque, E., Santiago, B., Pieres, A., et al. 2018, MNRAS, 478, 2006

Manwadkar, V., & Kravtsov, A. V. 2022, MNRAS, 516, 3944

Martin, N. F., Jungbluth, V., Nidever, D. L., et al. 2016, ApJL, 830, L10

Mau, S., Drlica-Wagner, A., Bechtol, K., et al. 2019, ApJ, 875, 154

Mau, S., Cerny, W., Pace, A. B., et al. 2020, ApJ, 890, 136

McDaniel, A., Ajello, M., Karwin, C. M., et al. 2023, arXiv e-prints, arXiv:2311.04982

Muñoz, R. R., Côté, P., Santana, F. A., et al. 2018, ApJ, 860, 66

Nadler, E. O., Wechsler, R. H., Bechtol, K., et al. 2020, ApJ, 893, 48

Pace, A. 2024, Local Volume Database, GitHub, , . https://github.com/apace7/local_volume_database

Pace, A. B., & Strigari, L. E. 2019, MNRAS, 482, 3480

Revaz, Y. 2023, A&A, 679, A2

Sawala, T., Frenk, C. S., Fattahi, A., et al. 2015, Monthly Notices of the Royal Astronomical Society, 456, 85. https://doi.org/10.1093/mnras/stv2597

Simon, J. D. 2019, ARA&A, 57, 375

Smith, S. E. T., Cerny, W., Hayes, C. R., et al. 2023, arXiv e-prints, arXiv:2311.10147

Steigman, G., Dasgupta, B., & Beacom, J. F. 2012, Phys. Rev. D, 86, 023506. https://link.aps.org/doi/10.1103/PhysRevD.86.023506

Torrealba, G., Belokurov, V., & Koposov, S. E. 2019, MNRAS, 484, 2181

Willman, B., Blanton, M. R., West, A. A., et al. 2005, AJ, 129, 2692

Wood, M., Caputo, R., Charles, E., et al. 2017, PoS, ICRC2017, 824